

The t - t' - J model in one dimension using extremely correlated Fermi liquid theory and time dependent density matrix renormalization group

Peizhi Mai¹, Steven R. White² and B. Sriram Shastry¹

¹Physics Department, University of California, Santa Cruz, CA 95064

²Department of Physics and Astronomy, University of California, Irvine, CA 92717

(Dated: June 26, 2018)

We study the one-dimensional t - t' - J model for generic couplings using two complementary theories, the *extremely correlated Fermi liquid theory* and *time dependent density matrix renormalization group* over a broad energy scale. The two methods provide a unique insight into the strong *momentum dependence* of the self-energy of this prototypical non-Fermi liquid, described at low energies as a Tomonaga-Luttinger liquid. We also demonstrate its intimate relationship to spin-charge separation, i.e. the splitting of Landau quasi-particles of higher dimensions into two constituents, driven by strong quantum fluctuations inherent in one dimension. The momentum distribution function, the spectral function, and the excitation dispersion of these two methods also compare well.

I. INTRODUCTION

In varying dimensions the t - J model continues to attract attention owing to its relevance in cuprates and other important strongly interacting electronic systems. The model embodies very strong correlations, which lie outside the regime of validity of perturbation theory, and thus pose a challenging problem. Our main goal in this work is to obtain an understanding of the properties in one dimension (1-d), *over a wide energy range*.

At low energies the bosonization technique has been widely applied to the (closely related) Hubbard model¹⁻⁵. For large U several non-perturbative methods have been devised to study the t - J model for general dimensions, including the study of finite clusters^{6,7} and large- N based slave particle mean-field theories⁸. In 1-d we also have exact results using Bethe's ansatz⁹⁻¹⁴ at special values of the parameters of the model, and also for long-ranged versions¹⁵ of the t - J model, using techniques developed in the Haldane-Shastry models. Photoemission experiments¹⁶ have been carried out to study the spectral properties of several quasi 1-d metals, relevant to the t - J model.

To study a wider energy range, including the low to intermediate and high energy regimes, we employ and compare the results from two complementary techniques. In 1-d, the density matrix renormalization group (DMRG)¹⁷ provides nearly exact results for the ground state, and can also be used for finite temperature and spectral properties. Ground state DMRG has been used to give the phase diagram of the t - J model over a broad range of parameters in¹⁸. Here we study dynamics using the time dependent density matrix renormalization group (tDMRG). tDMRG^{17,19} has been used to obtain virtually exact spectral functions for spin chains, but only a few times for doped Fermi systems. One such time was a tDMRG treatment of the t - J model, obtaining spectral functions for the system at finite temperature²⁰. In this work we use tDMRG only at $T = 0$, but we have pushed much farther in terms of system size, accuracy, and frequency resolution than in²⁰. This accuracy is needed to

resolve the detailed features of the self-energy, which has not been done before with tDMRG.

The other technique used is the extremely correlated Fermi liquid (ECFL) theory²¹. This analytical theory, which can treat a large class of large U problems, including the t - J model, uses Schwinger's functional differential equations for the electron Green's function. These equations are systematically expanded in a parameter $\lambda \in [0, 1]$, representing partial Gutzwiller projection. The $\mathcal{O}(\lambda^2)$ theory leads to a closed set of coupled equations^{21,22} for the Green's function. This treatment has been benchmarked in high dimensions and in 2-d. In infinite dimensions, dynamical mean field theory (DMFT)²³ provides a solution to the Hubbard model, and ECFL has been benchmarked recently^{24,25} against exact results from the single impurity Anderson model, and DMFT in $d = \infty$ ^{26,27}. The limiting case $U = \infty$ has been explored in detail in²⁸. The agreement at low energies is good enough to yield accurate results for the low T resistivity, a highly sensitive variable. In 2-d, ECFL has been applied recently to cuprate superconductors^{29,30}. It is therefore interesting to see how well this scheme deals with the physics of 1-d. The equations used here have the character of a skeleton graph series. We have checked that the second order skeleton graphs for the Hubbard model in 1-d already displays characteristics of spin-charge separation and non-Fermi liquid spectral functions, while the non-skeleton, i.e. bare perturbation theory does not.

Understanding the extent of *momentum dependence* of the Dysonian self-energy Σ in various dimensions is one of the goals of the present work. While the $d = \infty$ models have a momentum *independent* self-energy, momentum dependence of Σ is inevitable in lower dimensions. However there is a scarcity of reliable information on its extent and location. In most published work, the self-energy in 1-d is rarely presented³¹, or even calculated, since standard solutions directly deal with the Green's function. In contrast we focus on unraveling the (\vec{k}, ω) dependence of the Dysonian self-energy in 1-d and comparing with its higher dimensional counterparts.

arXiv:1712.05396v5 [cond-mat.str-el] 23 Jun 2018

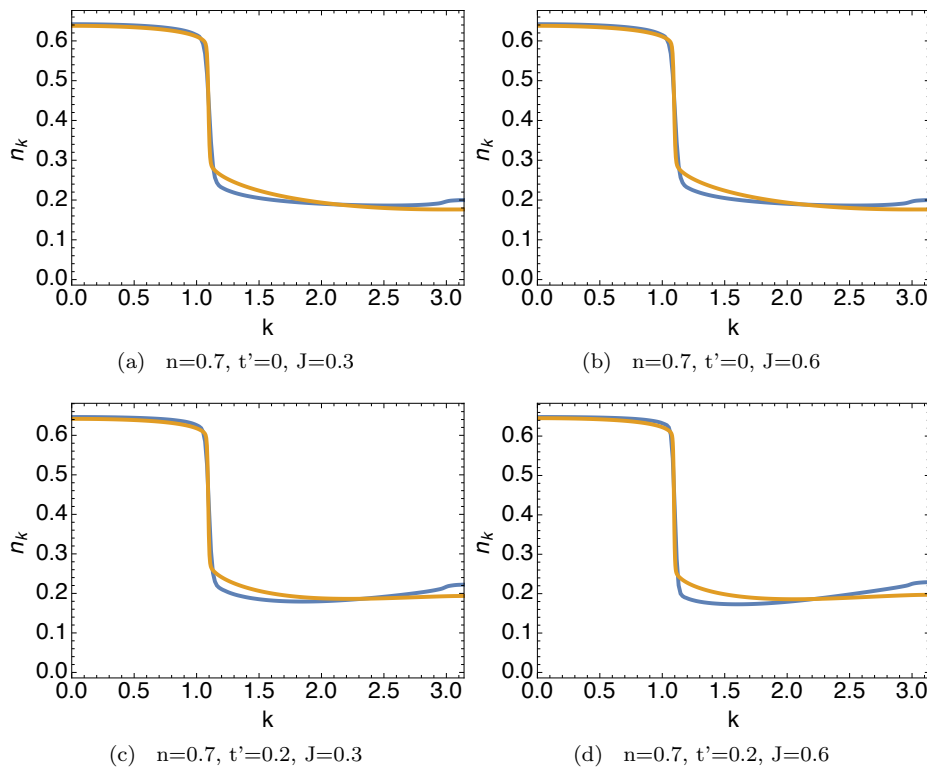


FIG. 1: Momentum distribution n_k for ECFL (yellow) at $T=0.005$ and tDMRG (blue) at $T=0$ with $n=0.7$, $J=0.3, 0.6$ and $t'=0, 0.2$. In all cases these two methods agree well especially in the occupied region and both give a power law singularity at k_F . The small discrepancy in the unoccupied region corresponds to the $3k_F$ feature in the exact solutions discussed in⁹. This subtle singularity is missed by the $\mathcal{O}(\lambda^2)$ equations.

II. OVERVIEW

In the present work we solve the $d = 1$ t - t' - J model for generic parameters using *the same set of ECFL equations* as in higher dimensions. We calculate from the two theories the momentum distribution function, self-energy, spectral function and excitation dispersion over a broad energy scale. In the low k, ω regime exhibiting non-Fermi liquid behavior, reasonable agreement is found between the two and the exact diagonalization (ED) data in the velocities of spinons and holons⁶, as well as the Tomonaga-Luttinger liquid (TLL) theory in anomalous exponent¹⁸. Extending the $\mathcal{O}(\lambda^2)$ ECFL equations to higher orders holds promise of a better agreement. At higher energies, where few studies exist, the agreement between the two theories is quite good already. A valuable insight gained at low energies is the close relationship between a momentum dependent ridge in the $\text{Im} \Sigma(k, \omega)$ and the spin-charge separation.

III. MODEL AND PARAMETERS USED

The Hamiltonian of the 1-d t - t' - J model is

$$H_{t,J} = -t \sum_{\langle ij \rangle} X_i^{\sigma 0} X_j^{0\sigma} - t' \sum_{\langle\langle ij \rangle\rangle} X_i^{\sigma 0} X_j^{0\sigma} - \mu \sum_i X_i^{\sigma\sigma}, \quad (1)$$

$$+ J \sum_{\langle ij \rangle} \left(\vec{S}_i \cdot \vec{S}_j - \frac{1}{4} X_i^{\sigma\sigma} X_j^{\sigma'\sigma'} \right),$$

where repeated spin indices are summed, $X_i^{\sigma 0} = P_G C_{i\sigma}^\dagger P_G$, $X_i^{0\sigma} = P_G C_{i\sigma} P_G$, $X_i^{\sigma\sigma'} = P_G C_{i\sigma}^\dagger C_{i\sigma'} P_G$ with $P_G = \prod_i (1 - n_{i\uparrow} n_{i\downarrow})$ as the Gutzwiller projection operator. $\langle ij \rangle$ and $\langle\langle ij \rangle\rangle$ refers to summing over first and second neighbor pairs respectively.

For this model^{21,29} we compute the results from the two theories at density $n = 0.7$, second nearest neighbor hopping $t'/t = 0, 0.2$ and $J/t = 0.3, 0.6$. We avoid the special cases of $t' = 0 = J$ since this leads to a degenerate spectrum, with a charge sector that is isomorphic to the spinless Fermi gas. The ECFL results are shown at various T while the tDMRG results are at $T = 0$ where most reliable calculations are possible. $t = 1$ is the energy unit and will be neglected below.

The tDMRG methods used are very similar to those used in Ref. [32]. We start by obtaining the ground state

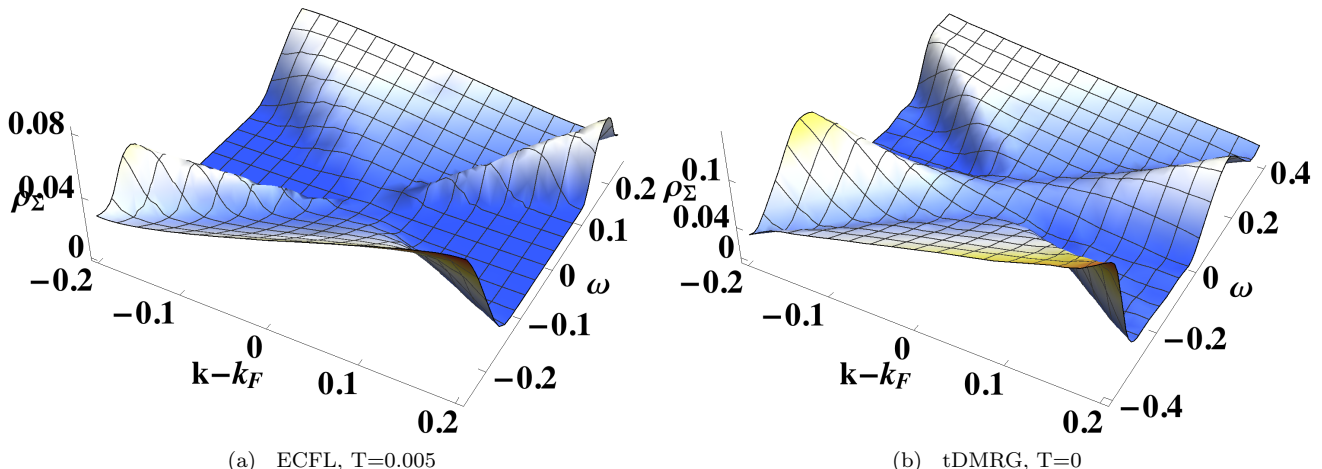


FIG. 2: $n=0.7$, $J=0.3$, $t'=0$: Imaginary self-energy $\rho_{\Sigma}(k, \omega)$ at low ω and $k - k_F$ from both methods. Both give a dominant (k, ω) dependent ridge running from left to right, and a less prominent feature running from top-left to bottom-right. Both of them pass through $k = k_F, \omega = 0$ region. The dominant ridge is responsible for the appearance of the twin peaks structure in the spectral functions which represents the spin-charge separation. The peaks for $k < k_F, \omega < 0$ are seen in the left half of the electronic spectral function in Fig. (6) panels (a,b), while the peaks for $k > k_F, \omega > 0$ are seen in the right half of the same figures. As seen in Fig. (5) panel (c), the peak in the self-energy ρ_{Σ} directly leads to a dip in the electronic spectral function ρ_G , provided the real part is small.

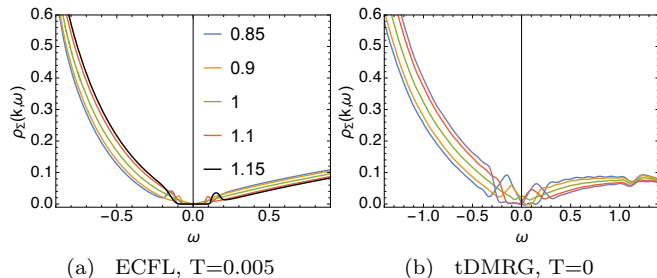


FIG. 3: $n = 0.7, J = 0.3$: $\rho_{\Sigma}(k, \omega)$ vs ω at marked k/k_F 's, from ECFL at $T = 0.005$ (a) and tDMRG at $T = 0$ (b) in a large scale. The two sets of results are similar on a broad energy scale, and are comparable to higher dimensional results. The low energy behavior is discussed below.

$|0\rangle$ using DMRG on a rather long but finite chain, with $L = 400$, and then apply \hat{c}_0 or \hat{c}_0^\dagger to a site 0 near the center, forming $|\psi(t=0)\rangle$. We use a Trotter based time evolution algorithm, with fermionic swap gates to handle next-nearest neighbor terms. We specify a density matrix eigenvalue truncation cutoff of 3×10^{-8} during the evolution, subject to a constraint on the maximum number of states kept of $m = 3000$. (Results were checked by comparing to $m = 2000$.) We evolve out to a time $t = 50$. At $t = 50$, the normalization of $|\psi(t)\rangle$ had decreased by a few percent, a small error affecting primarily the widths of any sharp peaks. The space and time dependent Green's function is obtained by sandwiching \hat{c}_i or \hat{c}_i^\dagger between the ground state and $|\psi(t)\rangle$ for all i . Linear

prediction is used to extend the time dependent Green's function out to $t = 100$, after which the data is windowed and Fourier transformed. This calculation represents the most accurate and detailed study to date of the spectral properties of the model at $T = 0$.

IV. MOMENTUM DISTRIBUTION FUNCTION

In 1-d t - J model, n_k shows a power law singularity at $k_F^{2,5}$, a signature of the TLL, unlike a jump in higher dimensions as Fermi liquid behavior. This feature is observed from both methods in Fig. (1) for different t' and J . Due to the second order approximation, the weak $3k_F$ singularity related to shadow band^{9,12} is not observed in ECFL results. Besides this weak effect, n_k from both methods agrees well, especially in the occupied side, showing that ECFL describes the correct t' and J dependent behaviors.

V. SELF-ENERGY

Next we present the Dysonian self-energy in terms of its spectral function ρ_{Σ} defined as

$$\rho_{\Sigma}(k, \omega) = -\frac{1}{\pi} \text{Im} \Sigma(k, \omega). \quad (2)$$

It is derived separately from the Green's functions in ECFL and tDMRG methods. In tDMRG, Σ can be found from G by inverting the Dyson relation $G^{-1} = G_0^{-1} - \Sigma$.

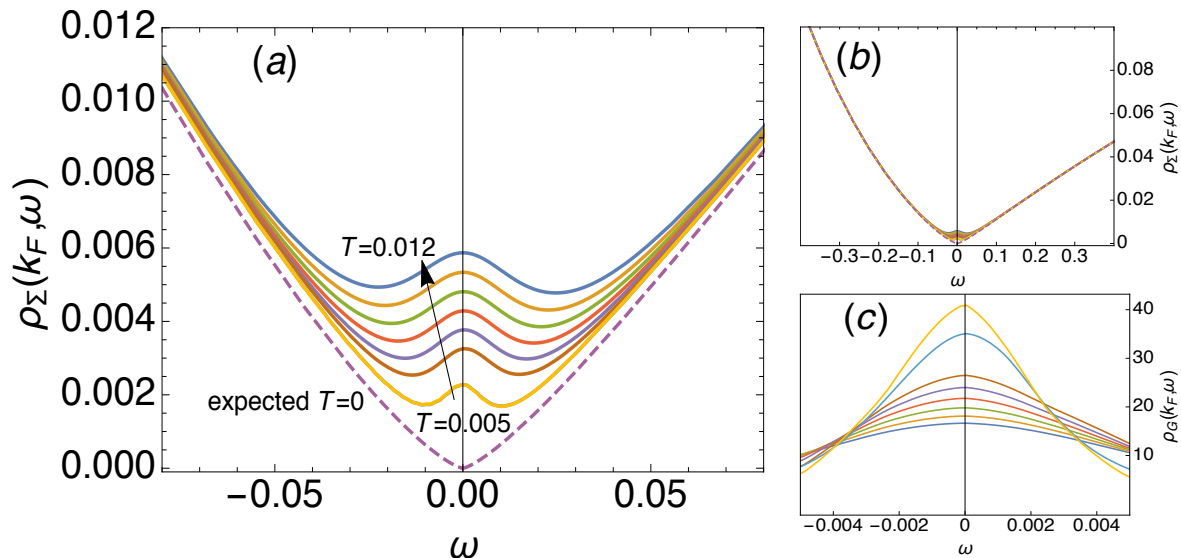


FIG. 4: $\rho_{\Sigma}(k_F, \omega)$ from ECFL is shown in (a) for several T at $J = 0.3, t' = 0$. The central peak $\rho_{\Sigma}(k_F, 0)$ scales as $T^{1.1}$, in contrast to Fermi liquid behavior T^2 . Extrapolating to $T = 0$ the double minimum structure disappears, leaving behind a $\sim |\omega|^{1.3}$ dependence. (b) displays the self-energy in larger scale where changing T barely makes a difference. (c) shows the spectral function softened by warming.

The ECFL theory produces two (non Dysonian) self energies Φ, Ψ^{21} , and the resulting G can again be inverted to find the standard Dysonian Σ . Both ECFL ($T = 0.005$) and tDMRG ($T = 0$) self-energies are shown in Fig. (2) for comparison.

In Fig. (2), the two theories have a similar pattern of k dependence, a dominant ridge running from left to right, and a less prominent feature running from top-left to bottom-right. They pass through $k = k_F, \omega = 0$ region. The ridge leads to the appearance of twin peaks in the spectral functions representing spin-charge separation. In the higher energy region in Fig. (3), both theories agree well and are similar to their higher dimensional counterparts.

A powerful feature of ECFL theory is that it allows us to vary temperature without extra effort, at least in the low to intermediate temperature region. In Fig. (4), ρ_{Σ} at k_F is presented in several temperatures. The bump becomes higher with increasing temperature though no obvious change in larger scale (Panel (b)). This is expected because warming softens the peak height of spectral function at k_F , which is $\rho_G(k_F, 0) = 1/(\pi^2 \rho_{\Sigma}(k_F, 0))$ in Panel (c). The central peak height $\rho_{\Sigma}(k_F, 0)$ scales as T^{α} with $\alpha \approx 1.1$, as opposed to $\alpha = 2$ expected for a Fermi liquid. Although $T = 0.005$ is the lowest temperature in the current numerical scheme for second order ECFL due to the finite lattice size (up to $L = 2417$ and

$N_{\omega} = 2^{17}$), we extrapolate the curve to $T = 0$. The peak at k_F disappears at zero T , and is replaced by a minimum at the origin corresponding to a singular peak in the spectral function, consistent with earlier studies^{2,12}. The self-energy approaches zero as $|\omega|^{\gamma}$, where $\gamma \approx 1.3$. This behavior is difficult to observe in our present tDMRG implementation, because the finite time cut-off, leads to a broadening. The peak and its k dependence is recovered on moving away from k_F , causing spin-charge separated peaks at $T=0$.

VI. SPECTRAL FUNCTION

We also compare the spectral functions from both methods. In Fig. (5) panel (a,b) both show a single peak at k_F and double peaks away from k_F representing spinons and holons respectively. Panel (c) puts together the spectral function away from k_F and different parts of its formula:

$$\rho_G(k, \omega) = \frac{\rho_{\Sigma}(k, \omega)}{[\omega + \mu - \varepsilon_k - \text{Re}\Sigma(k, \omega)]^2 + \pi^2 \rho_{\Sigma}^2(k, \omega)}, \quad (3)$$

It shows that $\omega + \mu - \varepsilon_k - \text{Re}\Sigma(k, \omega)$ is very small in the frequency range that spans the two peaks, and confirms that the visible twin peaks result from a peak in

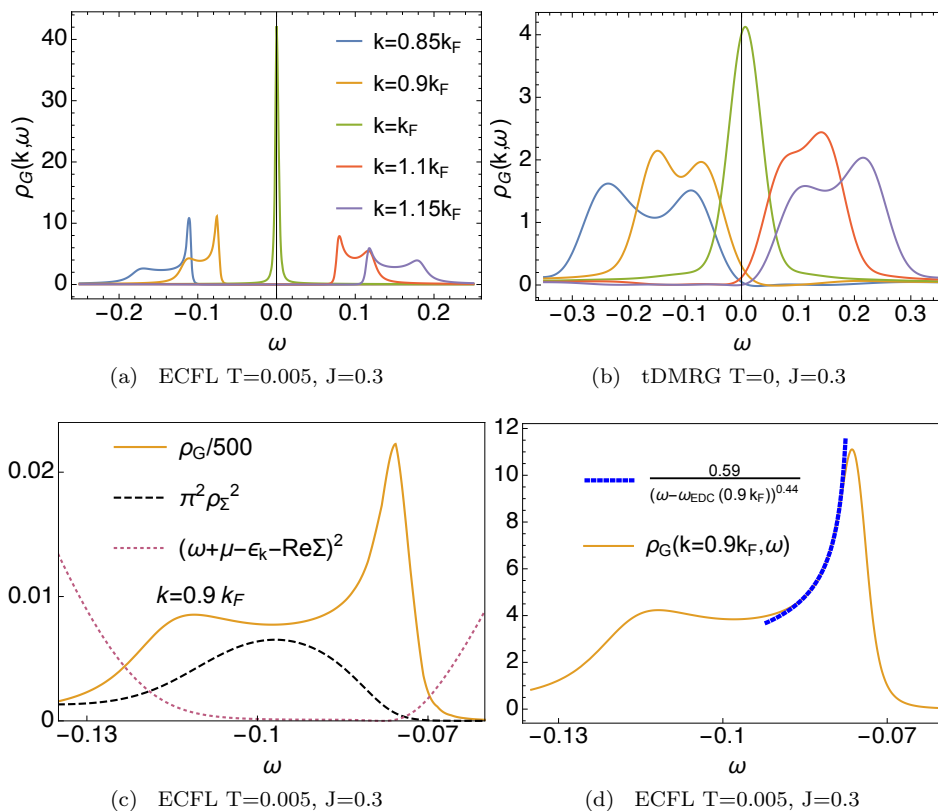


FIG. 5: Energy distribution curves (EDCs) at $t'=0$, $J=0.3$: (a) and (b) (same legends marking k/k_F) displaying the spinon and the holon for $k \neq k_F$. Panel (c) at $k = .9k_F$ shows that the peak in $(\pi\rho_\Sigma)^2$ (dashed black) coincides with the dip in the spectral function $\rho_G(\omega)$ (solid gold), while $(\omega + \mu - \epsilon_k - \text{Re}\Sigma)^2$ (magenta dots) is small everywhere. This implies that the twin peaks originate in the intervening peak of self-energy. Panel (d) also at $k = .9k_F$ shows the fitting procedure for finding the anomalous exponent $\zeta' \equiv \zeta - \frac{1}{2}$ for the spinon^{1,4}, we fit to $.59(\omega - \omega_{peak})^{\zeta'}$ (dashed blue), the best fit value is $\zeta' \sim -0.44$, close to the TLL result -0.45 ¹⁸.

ρ_Σ in the middle. Thus the location of the ridge lies in the minimum between spinon and holon peaks in the spectral function in panels (a,b), and in-fact the ridge causes the twin peaks. The exponents in panel (d) match reasonably with those from the TLL at $J = 0.3$ and also at 0.6 (where $\zeta' \sim -.49$ versus $\zeta' \sim -.46$ from Ref. [18]). We take the Luttinger parameter $K_\rho \approx 0.53$ at $J = 0.3, t' = 0$ from Fig. (4) in Ref. [18]. Then we calculate $\zeta = \gamma_\rho = (K_\rho + K_\rho^{-1} - 2)/8 \approx 0.05$ ^{1,4}. Therefore the anomalous exponent is $\zeta' = \zeta - \frac{1}{2} = -0.45$. The calculation is similar for $J = 0.6$ with $K_\rho \approx 0.56$ from Fig. (4). The tDMRG spectral function in panel b is too soft to extract the anomalous exponent, because its finite time cutoff leads to the broadening of spectral peaks in the low ω region.

In Fig. (6) we compares the spectral function of the tDMRG with the ECFL theory. The latter is presented both with and without Gaussian windowing by a suitable time constant comparable to that in our tDMRG work. As one might expect, the scales of the two theories differ if we compare the raw (un-windowed) figures, but become very close upon windowing.

VII. DISPERSION RELATION OF SPINONS AND HOLONS

We extract the excitation dispersion relation from spectral function in Fig. (7). According to Ref. [6], in the selected parameter region $n=0.7$, $J=0.3, 0.6$ and $t'=0, 0.2$, the holon velocity v_c is larger than the spinon velocity v_s . The error bars in the tDMRG originates from the broadening of the lines due to finite time windowing. Within the error bar, the DMRG agrees with the available ED data⁶. We expect that the neglected higher order terms in the ECFL theory would play a role in improving the holon velocity and also intensities.

VIII. CONCLUSION AND DISCUSSION

In this paper, we present the self-energy for the 1-d t - t' - J model from both ECFL and tDMRG and specify its characteristic low energy strongly momentum-dependent cross-ridge, qualitatively different from higher dimensional cases, responsible for the spin-charge separation

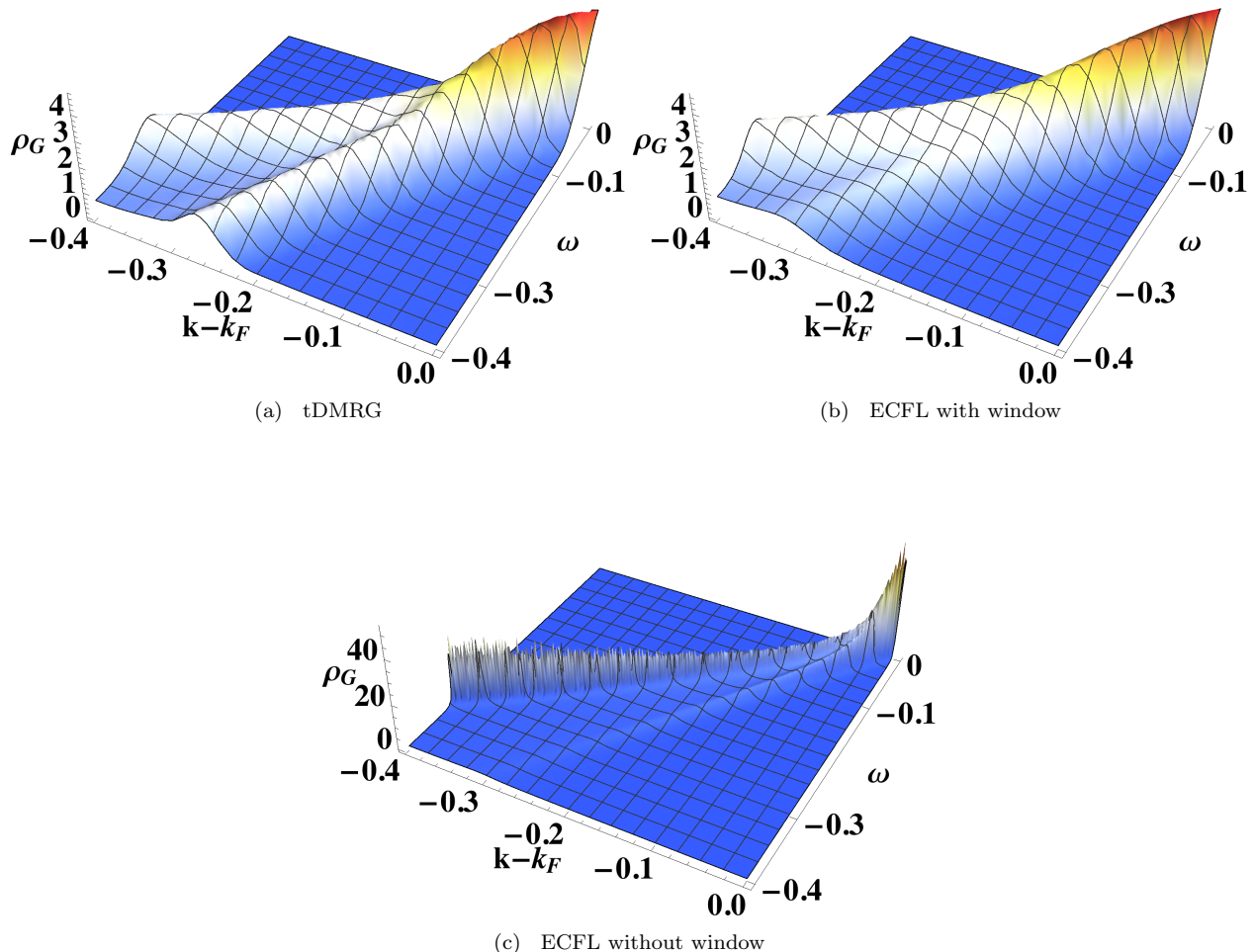


FIG. 6: $J = 0.6, t' = 0$. The spectral function of the tDMRG ($T = 0$) with an intrinsic time window (a) and the ECFL ($T = .005$) with (b) and without (c) a comparable time window. The introduction of a time window brings the two theories to the same scale. The central peak and the spinon peaks are of comparable height while the holon peak of ECFL is less prominent due to second order approximation.

in spectral function. This perspective is different from the ones discussed in earlier studies on this model in 1-d^{5,6,9-14,18,20,33}. The existence of a ridge structure in the imaginary self-energy, represents a non-trivial exact statement about the momentum dependence of the 1-d model.

We also compare the spectral function, the excitation dispersion and the momentum distribution function between both methods. They agree qualitatively in the low energy region, both capturing clear signatures of the TLL and more quantitatively at larger energy scales where the system behaves like it does in higher dimensions.

In summary we have shown in this work that the ECFL equations capture the essential physics of 1-d systems, namely spin-charge separation and non-Fermi liquid Green's functions in parallel to the behavior displayed by the tDMRG solution. A remarkable conclusion of this

work is that ECFL theory works in the widely different regimes of infinite dimensions²⁴, two dimensions^{29,30} and 1-d. This observation lends support to the overall scheme in general dimensions as well.

IX. ACKNOWLEDGEMENT

We thank Rok Žitko for helpful comments on the manuscript. The work at UCSC was supported by the US Department of Energy (DOE), Office of Science, Basic Energy Sciences (BES), under Award No. DE-FG02-06ER46319. The work at UCI was supported by National Science Foundation (NSF) grant DMR-1505406. The ECFL Computations used the XSEDE Environment³⁴ (TG-DMR170044) supported by National Science Foun-

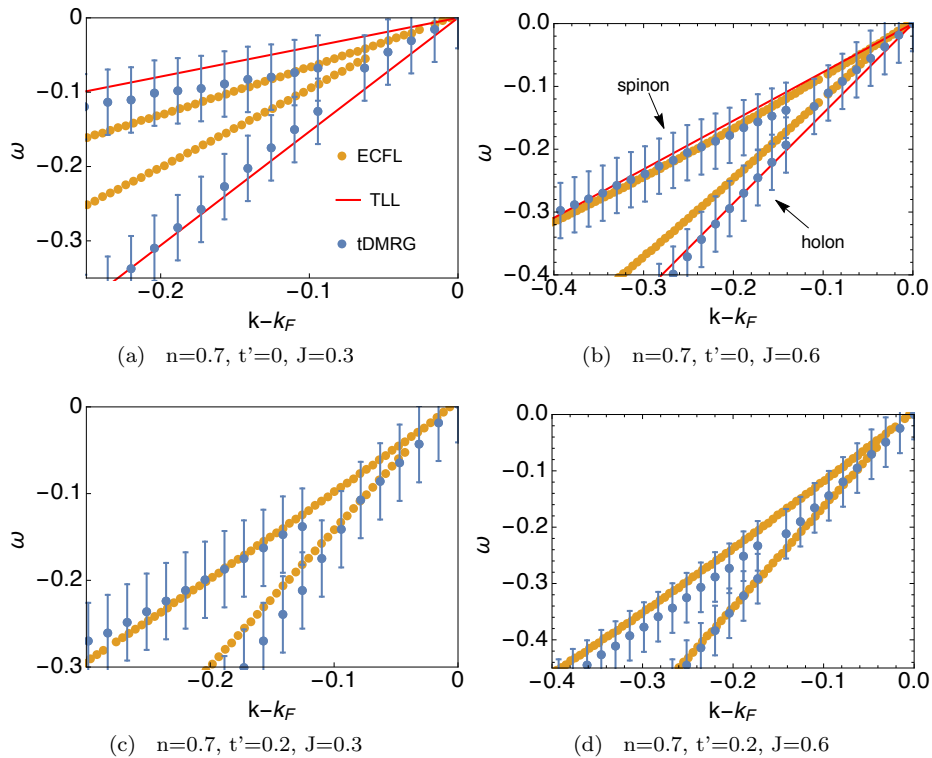


FIG. 7: Dispersion of excitations from both ECFL at $T=0.005$ (gold dots) and tDMRG at $T=0$ (blue dots), and the available ED data (red)⁶. The error bars in the tDMRG estimates are from the time window broadening. The tDMRG results are consistent with the ED results, while the ECFL holon dispersion deviates somewhat.

ation grant number ACI-1053575.

-
- ¹ T. Giamarchi, *Quantum Physics in One Dimension* (Oxford University Press, 2004).
- ² F. H. L. Essler, H. Frahm, F. Göhmann, A. Klümper and V. E. Korepin, *The One-dimensional Hubbard Model* (Cambridge University Press, Cambridge, England, 2005).
- ³ A. O. Gogolin, A. A. Nersisyan and A. M. Tsvelik, *Bosonization and Strongly Correlated Systems* (Cambridge University Press, Cambridge, England, 1998).
- ⁴ V. Meden and K. Schönhammer, Phys. Rev. B **46**, 15753 (1992); K. Schönhammer and V. Meden, Phys. Rev. B **47**, 16205 (1993); J. Voit, Phys. Rev. B **47**, 6740 (1993).
- ⁵ M. Ogata, T. Sugiyama and H. Shiba, Phys. Rev. B **43**, 8401 (1991); K. Penc and J. Sólyom, Phys. Rev. B **47**, 6273 (1993);
- ⁶ M. Ogata, M. U. Luchini, S. Sorella and F. F. Assaad, Phys. Rev. Lett. **66**, 2388 (1991). We use the velocities data of the spinon and the holon from Fig. (1).
- ⁷ J. Jaklic and P. Prelovsek, Adv. Phys. **49** 1(2010).
- ⁸ S. E. Barnes, J. Phys. F **6**, 1375 (1976); P. Coleman, Phys. Rev. B **29**, 3035 (1984).
- ⁹ M. Ogata and H. Shiba, Phys. Rev. B **41**, 2326 (1990).
- ¹⁰ P. A. Bares and G. Blatter, Phys. Rev. Lett. **64**, 2567 (1990).
- ¹¹ P. A. Bares, G. Blatter, and M. Ogata, Phys. Rev. B **44**, 130 (1991).
- ¹² J. Favand, S. Haas, K. Penc, F. Mila, and E. Dagotto, Phys. Rev. B **55**, R4859 (1997); K. Penc, K. Hallberg, F. Mila, and H. Shiba, Phys. Rev. Lett. **77**, 1390 (1996); K. Penc, F. Mila, and H. Shiba, Phys. Rev. Lett. **75**, 894 (1995); K. Penc, K. Hallberg, F. Mila, and H. Shiba, Phys. Rev. B **55**, 15475 (1997).
- ¹³ A. Parola and S. Sorella, Phys. Rev. Lett. **64**, 1831 (1990). S. Sorella and A. Parola, J. Phys. Condens. Matter **4**, 3589 (1992); A. Parola and S. Sorella, Phys. Rev. B **45**, 13156 (1992); Y. Ren and P. W. Anderson, Phys. Rev. B **48**, 16662 (1993).
- ¹⁴ H. Frahm and V. E. Korepin, Phys. Rev. B **42**, 10553 (1990); N. Kawakami and S. K. Yang, Phys. Lett. A **148**, 359 (1990).
- ¹⁵ Y. Kuramoto and H. Yokoyama, Phys. Rev. Lett. **67**, 1338 (1991); N. Kawakami, Phys. Rev. B **46**, 1005 (1992).
- ¹⁶ B. Dardel *et al.*, Phys. Rev. Lett. **67**, 3144 (1991); Y. Hwu *et al.*, Phys. Rev. B **46**, 13624(R) (1992); C. Coluzza *et al.*, Phys. Rev. B **47**, 6625 (1993); B. Dardel *et al.*, Europhys. Lett. **24**, 687 (1993); M. Nakamura *et al.*, Phys. Rev. B **49**, 16191 (1994).
- ¹⁷ S. R. White, Phys. Rev. Lett. **69**, 2863 (1992); Phys. Rev. B **48**, 10345 (1993).
- ¹⁸ A. Moreno, A. Muramatsu and S. R. Manmana, Phys. Rev. B **83**, 205113 (2011).

- ¹⁹ S. R. White and A. E. Feiguin, Phys. Rev. Lett. **93**, 076401 (2004); A. Daley, C. Kollath, U. Schollwoeck, and G. Vidal, J. Stat. Mech.: Theory Exp.2004, P04005.
- ²⁰ A. E. Feiguin and G. A. Fiete, Phys. Rev. B **81**, 075108 (2010).
- ²¹ B. S. Shastry, arXiv:1102.2858, Phys. Rev. Letts. **107**, 056403 (2011).
- ²² B. S. Shastry, arXiv:1312.1892, Ann. Phys. **343**, 164-199 (2014); (Erratum) Ann. Phys. **373**, 717 (2016).
- ²³ A. Georges, G. Kotliar, W. Krauth, and M. J. Rozenberg, Rev. Mod. Phys. **68**, 13 (1996).
- ²⁴ B. S. Shastry and E. Perepelitsky, arXiv:1605.08213, Phys. Rev. B **94**, 045138 (2016); B. S. Shastry, E. Perepelitsky and A. C. Hewson, arXiv:1307.3492, Phys. Rev. B **88**, 205108 (2013); E. Perepelitsky and B. S. Shastry, Ann. Phys. **357**, 1 (2015).
- ²⁵ W. Ding, R. Žitko, P. Mai, E. Perepelitsky and B. S. Shastry, arXiv:1703.02206v2, Phys. Rev. B **96** 054114 (2017); W. Ding, Rok Žitko, and B. Sriram Shastry, arXiv:1705.01914, Phys. Rev. B **96** 115153 (2017).
- ²⁶ X. Deng, J. Mravlje, R. Žitko, M. Ferrero, G. Kotliar and A. Georges, Phys. Rev. Lett. **110**, 086401 (2013).
- ²⁷ W. Xu, K. Haule, and G. Kotliar, Phys. Rev. Lett. **111**, 036401 (2013).
- ²⁸ R. Žitko, D. Hansen, E. Perepelitsky, J. Mravlje, A. Georges and B. S. Shastry, arXiv:1309.5284, Phys. Rev. B **88**, 235132 (2013).
- ²⁹ B. S. Shastry and P. Mai, arXiv:1703.08142, New Journal of Physics **20**, 013 027(2017); D. Hansen and B. S. Shastry, Phys. Rev. B **87** 245101 (2013).
- ³⁰ P. Mai and B. S. Shastry, in preparation.
- ³¹ V Zlatic and B Horvatic, Phys. Scr. T **39**, 151 (1991).
- ³² S. R. White, D. J. Scalapino, and S. A. Kivelson, Phys. Rev. Lett. **115**, 056401 (2015).
- ³³ R. Preuss, A. Muramatsu, W. von der Linden, P. Dieterich, F. F. Assaad, W. Hanke, Phys. Rev. Lett. **73**, 732 (1994).
- ³⁴ J. Town et al., "XSEDE: Accelerating Scientific Discovery", Computing in Science & Engineering, Vol.16, No. 5, pp. 62-74, Sept.-Oct. 2014, doi:10.1109/MCSE.2014.80